

Analysis of In-Situ Elastic properties of Fault Zones

Final Report for USGS Contract 02HQGR0012

James P. Evans

Department of Geology, Utah State University, Logan, Utah, 84322-4505

Project Summary

We characterize the geophysical properties of fault-related rock samples from the 80-100 m wide Mozumi fault zone, north-central Honshu, Japan. The fault is exposed in a research tunnel 300-400 m below the ground and we combine geological data with borehole geophysical logs to determine the elastic and seismic properties of the fault zone. Detailed mapping within the tunnel reveals that the fault zone consists of two zones of breccia to foliated cataclasites 20 and 50 m thick. Two narrow [10's cm wide] principal slip zones on which most of the slip occurred bound the central fault zone. The dominant deformation mechanisms within the fault zone were brittle fracture, brecciation, slip localization, plastic deformation, and vein formation in a sericite-calcite rich matrix. Clay alteration patterns are complex within the fault zone, with clay-rich fault breccia enriched in smectite, illite, and kaolinite relative to the kaolinite and illite dominant in the host rock. The fault zone exhibits depressed electrical resistivity values by 10-100 ohm-m relative to the wall rock, values of V_p and V_s values that ~ 0.30 km/s and ~ 0.40 km/s [10-20 %] less than protolith values. The spontaneous potential logs indicate the fault zone has increased freshwater content relative to formation waters. Well-bore based measurements of V_p and V_s in fault-related rocks to enable us to calculate values of Young's modulus from 16.2 to 44.9 GPa and Poisson's ratio for the fault zone of 0.263 to 0.393. The protolith Young's modulus of 55.4 GPa and a Poisson's ratio of 0.242. Lowest calculated values of Young's modulus and highest calculated values of Poisson's ratio correspond to fault breccia with increased porosity, high fluid content, and low resistivity values. Taken together, these data show that the shallow portion of the Mozumi fault consists of a complex zone of anastomosing narrow slip zones that bound broad zones of damage. Fluid-rock alteration and deformation created altered fault-related rocks, which has resulted in overall reduced interval velocities of the fault zone. These data indicate that seismic waves traveling along the interface or internally reflected in the fault zone would encounter rocks of differing and reduced elastic properties relative to the host rocks, but that in detail, material properties within the fault may vary.

INTRODUCTION

Determining the composition and structure of fault zones at all levels of the crust is an important element in understanding a variety of deformation and fluid-flow processes in the crust, including how faults affect fluid flow, how slip and damage is distributed within a fault, and how seismic energy is distributed during an earthquake. Addressing the questions posed above requires that we determine physical properties of fault-related rocks, and determine how these properties came to be.

A popular model of fault zone structure is the "Chester model" (Chester and Logan, 1986; Chester et al., 1993) in which a fault is represented as a core of highly sheared rock, embedded within a damage zone of fractured and faulted rock. While appropriate for a class of faults, the Chester model should likely be modified for other types of faults. In fine-grained sedimentary rocks for example, significant deviations from the Chester fault model zone may occur [Erickson, 1994; Warr and Cox, 2001; Yan et al., 2001; Heermance et al., 2003; Holland et al., 2006; Faulkner et al., 2003]. Faults in phyllosilicate-rich and clay-rich rocks (Rutter et al., 1986; Keller et al., 1995) may exhibit thick broad zones of damaged rock, punctuated by an anastomosing network of gouge zones. Slip is interpreted to be accommodated on numerous narrow slip zones that lie within the broad zone of deformation.

Fault-zone properties and structure can also be investigated with a variety of inversion methods of fault zone waves (Ben-Zion, 1998; Ben-Zion and Sammis, 2003; Li et al., 1999; 2004; McGuire and Ben-Zion, 2005). The temporal variations in fault zone properties can examine fault healing (Li et al., 2003), and analyses of fault-zone properties contribute to evaluating earthquake hazards along fault zones (Spudich and Olsen, 2001). Geologic observations can be merged with geophysical studies of fault zone structure and composition to help constrain the properties of the fault zone over a range of scales (Blakeslee et al.,

1989; Gettemy et al., 2004) that in turn can be used to examine the seismological structure of a fault and its impact on propagation of seismic waves. Many of the physical properties within fault zones at *in situ* conditions are difficult to resolve, but are critical for evaluating fault zone processes, such as the transmission and internal reflection of seismic energy [Spudich and Olsen, 2001; Gettemy et al., 2004] and the distribution of and frequency content of seismic energy that may travel within a fault zone (Li and Vidale, 1996). Direct measurement of elastic and seismic properties is difficult, owing to the friable nature of many fault-related rocks in the field and the difficulty of drilling into and retrieving samples from core. Gettemy et al. [2004] used P-wave seismic methods to infer the structure and petrophysical properties of an exposed fault zone, and showed that the internal structure of large strike slip faults can be complex, with regions of low seismic velocity and high anisotropy. Estimates of the seismic velocity contrasts across faults, using a variety of inversion schemes, range from 5% to more than 30%, depending on the location, depth, and resolution of the imaging method (Eberhart-Phillips & Michael, 1998; McGuire & Ben-Zion, 2005; Thurber et al., 2006; Hardebeck et al., 2007). We examine the material properties of fault-zone materials measured *in situ*, the processes that might cause these material property variations, and the textures in the rocks produced by these processes.

In order to evaluate the *in situ* petrophysical properties and near-surface structure of a fault zone, we present results of a study of the composition, structure, physical properties, textures, and fluid-rock interactions of rocks from a fault zone sampled at ~400 m below the ground surface in western Japan. Rock samples from drilled core associated with the Active Fault Survey Tunnel [AFST] and continuous borehole geophysical logs are combined with data on porosity and permeability to document the variations in fault zone properties across the fault. We discuss the results in light of a recent study of inversion of fault zone waves in the Mozumi fault (Mamada et al., 2004; Mizuno et al., 2004) and *in situ* hydraulic tests (Nohara et al., 2006) to document the relationship between deformation mechanisms, alteration, and elastic properties of the fault zone. This work provides data on the *in-situ* chemical, physical, and mechanical properties of the internal portion of an active fault in clastic sedimentary rocks in the upper portion of the crust, but at depths where weathering has not disturbed the textures and structures associated with faulting and fluid flow. The AFST also provides exposures of a fault at depths where seismic energy is transmitted to the surface, but above the region in which seismic energy is radiated. Analysis of the Mozumi fault zone exposed in the Active Fault Survey Tunnel provides a unique opportunity to merge geochemical, mineralogic, and petrophysical studies of fault-related rocks (this study) with results of hydrologic properties testing (Forster et al., 2003) and fault-zone guide wave studies (Mizuno et al., 2004) to determine the nature of the fault-zone scale variability of petrophysical properties and their causes.

Geologic setting

The Mozumi fault [MF] is a northeast-striking, right-lateral strike-slip fault in north-central Japan with 125-500 m of slip (Figure 1; Ando, 1998). The research tunnel excavated by the Terrestrial Subsurface in Earthquake Frontier Project at ~300-400 m below the surface trace of the fault intersected the Mozumi fault to provide direct access and observation of this active, clay-rich fault zone over 200 m across the fault zone and host rocks (Figure 2). The Mozumi fault zone is 80-100 m wide and is an example of a complex, heterogeneous fault zone in sedimentary rocks (Mamada et al., 2002, 2004; Forster et al., 2003; Mizuno et al., 2004; Nohara et al., 2006). In addition to the tunnel, samples were acquired from horizontal and 60° plunging boreholes that crossed the entire fault zone. The general geology of the region is summarized in Kawai and Nozawa, (1959), Soma and Akiyama (1984) and Yamada et al., (1989). The Mozumi fault is 23 km long, branches northwest from the southeastern end of the Atotsugawa fault (Ando, 1998, Takeuchi and Ongirad, 2003), strikes ~N 50-60° E and has a near-vertical dip (Hirahara et al., 2003; Takeuchi and Ongirad, 2003). In the study area, the fault strikes ~N 40-45° E nearer the northwest termination of the Mozumi fault, where the fault appears to bend (Ito, 1999; Mizuno, 2004).

The Active Fault Survey Tunnel (AFST) project in Gifu prefecture, Japan, trends N 24° W for 481 m from an access point from a tunnel in the Kamioka Pb-Zn-Ag deposit (Mariko et al., 1996). The tunnel provided direct access of the Mozumi fault at a depth of 300-400 m (Figure 2; Shingu et al., 1997). Within the fault survey tunnel, the Mozumi fault cuts sandstone, shale, and siltstone of the middle Jurassic to lower Cretaceous Tetori Group. (Figure 2; see also Matsuda, 1966). The Tetori Group overlies Paleozoic Hida metamorphic rocks and Paleozoic-Mesozoic granite in the area. The Tetori Group consists of alternating conglomerate, fine to very coarse-grained sandstone, shale, siltstone, and coal seams (Fujita, 2002). These sedimentary rocks are also overlain by the Hida Gneiss along the Yokoyama thrust. The AFST was mapped by geologists of the Mitsui Mining and Smelting Co. as part of the development of the

tunnel for scientific research (Figure 2; Forster et al., 2003; Nohara et al., 2006). The map in Figure 2 is derived directly from the unpublished mine geologists data. Mine mapping along the tunnel, before it was lined revealed the presence of two damage zones, termed “crush zones” by the mine geologists. Zone A is ~20 m wide and is interpreted as the main trace of the Mozumi fault, and crush zone B is ~65 m wide and is interpreted as a subsidiary fault to the Mozumi fault (Forster et al., 2003). Hereafter, crush zone A is referred to as the Mozumi fault or primary damage zone. Adjacent to the damage zones line narrow clay-rich slip zones that appear to be 10-20 cm wide. Only of these zones was exposed during our work, but descriptions of these zones, translated from the Japanese report, (Shingu et al., 1997) indicates that the fault zones are characterized by clay gouge and fault breccia. The mine map also documents the presence of 6 thin fault zones, which are interpreted to be the loci of most of the slip within the zone (Nohara et al., 2006).

Except for a small window through the AFST lining, the only direct access to the fault-related rocks is in four cored and logged boreholes drilled off of the main tunnel (Figure 2). Borehole 1 was horizontal and intersected the largest subsidiary fault [zone B]. Boreholes A and 2 intersect the main trace of the Mozumi fault, and borehole A plunged 60° north-northwest from the horizontal Active Fault Survey Tunnel. Borehole 3 samples lithology outside of the fault zones northwest of the fault. Unoriented core samples of siltstone were collected from borehole A of the Active Fault Survey Tunnel (samples MZA-1 through MZA-10; Table 1). Three samples of undeformed medium- grained sandstone [MZ 1A] were collected from 26.9 m along borehole , and two siltstone samples [MZ-1] was collected 50.1 m from the southwest end of borehole 1. These samples are similar to the clasts of siltstone breccia in the fault zone, has similar bulk mineralogy, and are used to compare both the microstructures and geochemistry to samples from the Mozumi fault zone. We also use the mine mapping of the fault to evaluate the mesoscopic structure of the fault and host rock.

Mine geologists recorded the Rock Quality Designation (RQD), core recovery, and water inflow along the cored intervals for several of the boreholes that crossed the faults (Figure 3). The RQD scheme is a measure of rock integrity, which is defined as the percentage of core pieces in a given length of core that are twice the core diameter (Deere and Deere, 1987). The rock quality indices of rock masses surrounding the Mozumi fault range from 0-60%. A value of <25% indicates very poor rock quality, 25-50% indicates poor rock quality and 50-75% indicates fair rock quality. Rock quality is reported as 0- 10% across the “crush zones” of the Mozumi fault, reflecting a high degree of mesoscopic damage as determined by the mining geologists. Core recovery reflects the quality of the faulted rock, and significant fluxes of water were recorded at the main fault zone (Figure 3b).

Map-scale and mesoscopic structural data of borehole A were provided by Power Reactor and Nuclear Fuel Development Corporation (now Japan Atomic Energy Agency) from an internal report (Shingu et al., 1997). Orientations of fractures in borehole A (Figure 4) were measured for wall rock and Mozumi fault rock; however, few fractures were measured within the Mozumi fault zone because the rocks are brecciated, resulting in a small number of recognizable discrete fractures. Three main sets of fractures are seen (Figure 4): Fracture set 1 has a mean orientation of 155°, 20° and is at a mean angle of 82° to the main trace of the fault. Two nearly-vertical subsidiary fracture sets are oblique to the Mozumi fault: one with a mean orientation of 001°, 71° that makes a 42° angle with Mozumi fault (fracture set 2), and the other with a mean orientation of 063°, 74° that makes a 28° angle with the Mozumi fault (fracture set 3).

The undeformed Tetori Group rocks are a sequence of very fine- to fine-grained siltstone and fine- to coarse-grained sandstones with subrounded quartz grains in the fine-grained matrix. The fine-grained portions of the siltstone protolith are thinly to medium-bedded, and little deformation can be seen surrounding larger quartz grains. The sandstone sequence consists of fine- to coarse-grained, subangular to subrounded quartz and feldspar sandstones and arkoses. Microstructures of deformed rocks from a secondary fault in borehole A consist of siltstone cut by several veins and narrow faults containing clay films. The siltstone has a sericite-rich matrix, as well as calcite and phyllosilicates. Veins consist of fine-grained quartz at fracture walls that progressively coarsens inward and surrounds calcite vein fill.

The southeast edge of the fault zone consists of altered siltstone cut by a fault of unknown size. In hand sample, the fault makes a clear separation of heavily altered, indurated siltstone and highly comminuted clay-rich fault rock. The fault interface is smeared with tacky, green, chlorite-rich clay. Twinned calcite grains indicates plastic deformation and appears to have been injected into the rock because it is found in irregularly shaped, discontinuous zones that have sharp boundaries with surrounding quartz grains. Approaching the fault, quartz grain size decreases and additional mineral phases are present. Calcite is present nearest the fault, bordered by a zone of quartz and chlorite, and less deformed quartz, calcite, and

some feldspar are present. There are also radial growths of epidote and zoned quartz with stylonite-like sutures.

Bulk and Clay Mineralogy Bulk powder x-ray diffraction identifies quartz, feldspar, calcite, muscovite/illite, montmorillonite (smectite), kaolinite, and chlorite and/or vermiculite as the main mineral constituents in the samples. All samples contain illite/muscovite and kaolinite clays. Several samples from the primary damage zone contain smectite mixed with combinations of illite, kaolinite, and possibly chlorite or vermiculite (Table 2). Samples from the southeast edge of the primary damage zone as well as across the core of the fault contain smectitic clay mixed with illite/muscovite and kaolinite, and possibly small amounts of chlorite and R₀ I-S (disordered illite-smectite clay minerals). Samples from the northwest edge of the primary damage zone are composed of illite/muscovite and kaolinite. Chlorite or vermiculite and kaolinite-montmorillonite clays are present along the secondary fault at the northwest edge of the primary damage zone. The siltstone protolith contains illite/muscovite and kaolinite, and possibly a small amount of R₀ I-S. The relative amount of muscovite and illite in each sample is unknown, and these minerals have been considered as one mineral phase.

PETROPHYSICS OF FAULT-RELATED ROCKS

Six borehole geophysical logs were recorded for borehole A (Shingu et al., 1997). These logs have been projected to the horizontal (Figure 5) and were correlated to samples collected from borehole A for petrophysical analysis. These logs measure different physical responses and are useful in determining the bulk (1-10 m) properties of Mozumi fault rocks. The spontaneous potential (SP), natural gamma ray, and resistivity logs provide insights into the composition of the rocks, and the acoustic, sonic, and compressional and shear wave (V_p and V_s , respectively) logs provide direct measurement of the seismic properties. In addition, the ratio of the P-wave velocity to the S-wave velocity (V_p/V_s) is an indicator of the presence of fluids, with high values of V_p/V_s indicating high fluid content.

The wireline logs show that the fault zone has a variable signature, depending on the log examined. The most notable log signature associated with the fault zone is a reduction in the resistivity log (Figure 5). Rocks outside the fault zone have resistivities as high as 100 ohm-m, whereas within the fault zone, resistivity decreases to nearly 0, likely indicating the presence of water in the fault zone. Rocks southeast of the fault zone also demonstrate a similar reduction in shaly rocks. The fault zone signature is also seen in the SP log, where an increase is observed over the protolith, and a modest reduction of V_p and V_s .

The resistivity log records nearly the same response for long and short-range curves. Low resistivity values (0-50 ohm-m) indicating increased pore fluids are recorded across the Mozumi fault. A deflection from the SP shale baseline across the Mozumi fault may indicate a zone of enhanced permeability. The gamma-ray log indicates areas of naturally occurring radioactivity, or shale content, in the Mozumi fault, as do spot core logs and physical core available for this study. The sonic log shows slower velocities for shale or siltstone within the Mozumi fault zone than shale or siltstone outside of the fault zone, indicating porosity has been created within the fault zone.

The values of the shear wave and compression wave velocities are also slower across the Mozumi fault (1.99 ± 0.05 and 4.04 ± 0.06 km/s) relative to surrounding wall rock (2.36 ± 0.05 and 4.36 ± 0.08 km/s). A Mann-Whitney U test for comparison of two sample populations of non-parametric, open data was employed to test for statistical significance of the decrease in seismic velocity across the Mozumi fault zone. The null hypothesis of H_1 : velocities across the Mozumi fault zone \geq velocities of wall rock was rejected at a confidence interval of 95%. Thus the decrease in seismic wave velocity across the Mozumi fault zone is statistically significant. This indicates that fault-related activity and perhaps the alteration discussed above has significantly altered the physical properties of the Mozumi fault rocks relative to wall rock.

Calculations of Elastic Moduli and Porosity

We determine elastic moduli of rocks within the fault zone from seismic wave velocities recorded by wireline logs and the rock density. Density was measured for all samples collected from borehole A by simple displacement of water methods. The values of Lamé's constant λ , and the shear modulus μ (a measure of rigidity) can be calculated from:

$$V_s = \sqrt{\mu / \rho} \quad [1]$$

and

$$V_p = \sqrt{(K + 4/3\mu) / \rho} = \sqrt{(\lambda + 2\mu) / \rho} \quad [2]$$

where V_s is shear wave velocity from the wire line log, V_p is the compressional wave velocity from the wire line log, K is the bulk modulus, μ is the shear modulus, and ρ is calculated density (Kramer, 1996). Using λ and μ , Young's modulus (E) and Poisson's ratio (ν) can be calculated for borehole A samples using

$$E = (\mu(3\lambda + 2\mu)) / (\lambda + \mu) \quad [3]$$

and

$$\nu = \lambda / 2(\lambda + \mu) \quad [4]$$

(Kramer, 1996; Mavko et al., 1998). Thus we estimate the elastic properties of fault zone materials, and use these values in conjunction with observations of fault rock properties to infer the physical properties of the fault zone (Table 3).

Calculated values for Young's modulus and Poisson's ratio fall towards the high end or above experimentally derived values measured for intact samples of siltstone, shale, and sandstone (Figure 6; Haas, 1981; Szwilski, 1982; Hatheway and Kiersch, 1989; Wong et al., 1997). Laboratory values for seismic velocities and elastic moduli are often different than in-situ values due to biased sampling of un-fractured, undeformed, pure rock samples for laboratory testing (Stierman and Kovach, 1979; Sayed, 2001). This would result in faster seismic velocity, higher Young's modulus, and lower Poisson's ratio values for laboratory experiments with respect to *in situ* values. The Poisson's ratio determined here is indeed lower for experimentally derived values (average of 0.206) than values calculated from in-situ seismic velocities of the Mozumi fault zone (average of 0.320; Figure 10). The value of Young's modulus, however, is higher in the naturally deformed rocks (average of 29.9 GPa) than for experimental values (average of 20.5 GPa). Values of Young's modulus may be higher for Mozumi fault zone siltstone than for laboratory samples of sandstone, shale, and siltstone due to cementation and mineralization as observed in thin section (Figure 6), or due to the presence of interstitial (and incompressible) fluids in the fault (Forster et al., 2003). Mineralization may account for the stiffness of the fault rocks relative to pure sandstone and siltstone samples used in laboratory testing for Young's modulus.

The amount of clay in each sample was determined with a hydrometer in the Utah State University Soil Testing Laboratory (Table 4). Some error is introduced as small (<mm) pieces of siltstone breccia clasts did not completely disaggregate upon mixing. The hydrometer measures the density of soil (clay) colloids. Once the clay content is estimated for each sample, we can calculate porosity (ϕ) from the velocity data by

$$V_p = 5.77 - 6.94\phi - 1.73\sqrt{C} + 0.446(P_e - 1.0e^{-16.7P_e}) \quad [5]$$

where C is the clay volume fraction and P_e is the effective pressure in kilobars (Table 4; Eberhart-Phillips, 1989). The confining pressure at the tunnel depth of 350 m is 7.6 MPa (Forster et al., 2003) and we assume a hydrostatic gradient for the fluid pressure. The confining pressures for core samples were calculated using the true depth below the ground surface for each sample. Calculated porosity values from equation [5] are similar to calculated porosity values using the following equation derived by Castagna et al. (1985):

$$V_p = 5.81 - 9.42\phi - 2.21V_{cl} \quad [6]$$

where V_{cl} is the clay volume. Calculated porosity values are listed in Table 3. These relationships are derived from regressions of experimentally determined values of P_e , ϕ , V_{cl} , V_p , and V_s . An RMS curve fit is applied to the data (Eberhart-Phillips et al., 1989) so that a relationship between the velocities and physical properties is extracted.

The V_p / V_s values (Table 3) are a proxy for fluid content and porosity, with high V_p / V_s values indicating an increased presence of fluids and porosity (Stanchits et al., 2003). Portions of the Mozumi fault zone have high relative fluid content ($V_p / V_s = 2.19-2.38$) (Table 3), whereas some portions of the fault zone have lower values of V_p / V_s (1.77-1.95) and higher S-wave velocity values (2.00-2.55 km/s). Typical V_p / V_s

values for sandstone, shale, and siltstone range from 1.5 (dry sandstone) to ~2.5 (Castagna et al., 1985), and the velocity reduction calculated here for the fault zone is consistent with velocity reductions associated with clay and fluid content of rock (Klimentos and McCann, 1990; Wang and Nur, 1990).

We compare our calculated values of Poisson's ratio from our data to compilations for unfaulted siltstone and sandstones by Castagna et al. (1985) and to the analysis of similar rocks by Brocher (2005; Figure 11), in which Poisson's ratio is examined as a function of V_p . Most of the fault-related rocks examined here have values of ν that are higher than that of the global populations, and from [4], we infer that most of this increase is due to the decrease in m , the shear modulus of the rocks. We suggest that the higher porosity in the damage zone (Forster et al., 2003) and the fluid-rich clay alteration products documented here contribute to lower values of the shear modulus in parts of the fault zone, and thus lower values of V_s , while higher values of E are produced by the presence of pore fluids and/or cements.

DISCUSSION AND CONCLUSIONS

Mizuno et al. (2004) analyzed the Mozumi fault fault-zone-trapped waves produced from 9 earthquakes and recorded by a seismic array within the Active Fault Survey Tunnel to infer fault zone structure including total damage zone width, average S-wave velocity, and wave attenuation. They estimate the width of the fault zone to be 160-400 m, which corresponds to the damage zone observed by mine geologists in the Active Fault Survey Tunnel of ~200 m across the entire fault zone. The average shear wave velocity from the trapped wave study were 2.9-3.1 km/s, or ~1.0 km/s faster than the average value determined from the wire line log for Mozumi fault zone rocks. The seismic wave attenuation (Q_s) in the fault zone is 60-90, much lower than crustal Q values of ~160 (Anderson and Hart, 1978; Udias, 1999).

When combined with the result of our study, we can delineate the internal physical structure of the fault zone, and determine the chemical and mechanical processes responsible for the changes observed. Mamada et al. (2004) and Mizuno et al. (2004) provide analyses of the Mozumi fault zone over scales of 10's to 100's of meters, whereas our data provide data at the cm to 10's m scale. Their results indicate the fault zone is a region of lower V_p and V_s , with geometric complexities affecting the movement of the headwaves. The V_p and V_s values we determined from borehole A decrease from sandstone to shale to clay (Table 5; Figure 9; Shingu et al., 1997). In addition, seismic velocity values are decreased across the Mozumi fault relative to the wall rock (Table 5, Figure 9). The average P-wave and S-wave velocities determined from the seismic studies for protolith are 4.6-4.9 km/s and ~2.6 - 3.0 km/s, respectively (Mamada et al., 2004; Mizuno et al., 2004). Four types of fault zone structures are recognized, including fractures along borehole A, lithology changes, including clay composition, foliation and other microstructures, and heterogeneity of physical and mechanical properties (Forster, et al., 2003; this study). The wireline log data we present here (Figure 9) suggest a slightly higher V_p and agree well with respect to V_s . The ~ 20% reduction of velocities are a result of both deformation and fluid-rock interactions.

In detail, the relationships between geochemical, mineralogic, and physical properties of fault-related rocks are complex and variable across the fault zone. Portions of the fault zone are less dense, have low V_p/V_s values, low ν , and low resistivity values, have more clay content than other samples, and have the most depleted geochemical signatures. Interspersed with these deformed rocks are samples with high values of E (28.6 GPa and 31.0 GPa), low values of ν (0.264 and 0.263), and contain illite/muscovite and kaolinite clays. Low to intermediate fluid content ($V_p/V_s = 1.87, 1.89, \text{ and } 1.90$), high values of E (40.8-44.9 GPa, 35.0 GPa, and 30.9), intermediate values of ν (0.298-0.299, 0.306), and mixtures of clay types also occur. Overall fluid-rock interactions, as depicted in the geochemical data, are also variable across the fault zone. These data illustrate the heterogeneous nature of the physical properties within the fault zone. Fault rocks of the Mozumi fault have values of Young's modulus ~11-39 GPa lower than the protolith samples, and values of Poisson's ratio 0.151-0.021 higher than protolith samples (Table 3). These values indicate that, overall, the fault zone rocks are not as stiff and have a greater porosity than their protolith.

The abundance of veins throughout the Mozumi fault zone and numerous mineral phases present around the secondary fault indicate that fluid flow was active during and after fault motion. Veins that fill shattered grains indicate that fluids must have transported calcite and gouge into void spaces quickly before the fractures closed. Anastomosing gouge and irregular shaped blebs of coarse calcite crystals within the matrix indicate fluid pressurization and coseismic injection of fluids and saturated fault gouge. The available fluids that created these microstructures likely persisted after fault activity. Thin sections contain veins that show evidence for evolving fluids that precipitated quartz followed by calcite or chlorite.

Permeability and porosity reported by Forster et al. (2003) indicate that permeability (k) and porosity (n) values in siltstone protolith is on the order of 10^{-17} m^2 and 1.6%, respectively) and that the

smallest k values occur in clay-rich zones (10^{-18} to 10^{-19} m²), with intermediate values of k and n in fault breccia with clay gouge (10^{-14} to 10^{-16} m², 8-9%) and the largest k values for fractured rock without significant clay content (10^{-13} to 10^{-14} , Table 3). The values of porosity calculated from clay content and well-bore based P-wave velocity for fault rocks in this study are at least double the porosity values reported by Forster et al. (2003), whereas the values reported by Forster et al. (2003) measure connected porosity using the fluid injection method. Hydraulic conductivities determined from the in situ flow tests (Nohara et al. 2006) reveal a lithology and structural dependence on hydraulic conductivity, with values ranging from 10^{-6} to 10^{-7} m/sec.

Other data presented in this study, and recent work of others support an interpretation of the heterogeneous structure of the Mozumi fault (Forster et al., 2003; Nohara et al., 2006). Permeable zones of brecciated fault rock correspond to areas of low relative resistivity, high relative values of V_p/V_s , low values of E , and high values of ν (Figure 7). Fault-related rocks with lower values of V_p/V_s correspond to a greater percentage of clay, higher resistivity values, are more chemically altered than protolith, and these rocks have higher values of E , and have lower values of ν than the zones of permeable fault rock (Figure 7). The presence of smectite (as well as the geochemical alterations) indicates fluid-rock interactions, as the protolith is illite-siltstone. These observations suggest that pockets of fluid-rich rock may migrate through time, thus resulting in illite-smectite reactions and other alteration along the fault zone. The migration of fluid and resulting alteration may cause a gradual change in the behavior of the fault and the properties of that rock mass over time.

We suggest that our data support a model of a heterogeneous Mozumi fault zone with fault-parallel, fluid-rich zones that are mixed with clay-rich zones and subvertical slip zones. Similar complexity of borehole log signatures, composition, and physical properties has been noted in decollement faults associated with accretionary prisms (Shipley et al., 1995; Tobin and Moore, 1995) and in active strike-slip faults (Gettemy et al., 2004). In detail, faults in fine-grained sedimentary rocks appear to exhibit significant internal structural and compositional variability that is reflected at a variety of scales and in a variety of signatures.

CONCLUSIONS

- 1) The Mozumi fault-related rocks are altered and mineralized fault breccias with foliated sericite/muscovite-rich matrix that show evidence for concentrating shear and plastic deformation in the matrix. The Mozumi fault is a low velocity zone relative to wall rock in borehole A and protolith as determined from wireline logs of P-wave and S-wave velocities across the fault zone and seismic wave velocities of protolith as reported in Mizuno et al. (2004; references therein).
- 2) Fault rocks from the Mozumi fault zone have increased porosity (10-22%) relative to the protolith. Electrical and seismic properties, elastic moduli, porosity, permeability, fault-related textures, and clay content vary across the main fault zone. Rocks in which fluid-rock interactions were significant have low values of young's modulus and higher values of Poisson's ratio; fault breccias that have higher values of E , low to intermediate values of ν , and are more altered and contain more clay and intense microstructural deformation.
- 3) The attenuation factor Q , for the Mozumi fault zone is 60-90, whereas average crustal values are ~160 (Mizuno et al., 2004; see also Blakslie et al., 1989 for Q of faults). Combined with the microstructural and geochemical observations presented here, we suggest that these low Q values are a consequence of the accumulated effects of fault-related damage and fluid-rock alteration while the faults are active.

References

- Ando, M. (1998), Overview and purpose of the active fault probe at the Mozumi-Atotsugawa fault system (Progress Report), in *The International Workshop of Frontiers in Monitoring Science and Technology for Earthquake Environments*, Toki and Kamioka, Japan, November 1998, Japan Nuclear Cycle Development Institute Report TW7400 98-001.
- Bedrosian, P.A., M.J. Unsworth, G.D. Egbert, and C.H. Thurber (2004), Geophysical images of the creeping segment of the San Andreas Fault; implications for the role of crustal fluids in the earthquake process, *Tectonophysics*, 385, 137-158.
- Ben-Zion, Y. (1998), Properties of seismic fault zone waves and their utility for imaging low-velocity structures, *J. Geophys. Res.*, 103, 12,567-12,585. 1998.
- Ben-Zion, Y., and C. Sammis (2003), Characterization of fault zones, *Pageoph*, 160, 677-715.

- Blakeslee, S., P. Malin, and M. Alvarez, (1989), Fault-zone attenuation of high-frequency seismic waves, *Geophys. Res. Lett.*, *16*, 1321-1324.
- Brocher, T. M., (2005), Empirical Relations between Elastic Wavespeeds and Density in the Earth's Crust, *Bull. Seis. Soc. Am.*, *95*, 2081-2092.
- Caine, J.S., J.P. Evans, and C.B. Forster (1996), Fault zone architecture and permeability structure, *Geology*, *24*, 1025-1028.
- Castagna, J.P. M.L. Batzle, and R.L. Eastwood (1985), Relationships between compressional-wave and shear-wave velocities in clastic silicate rocks, *Geophysics*, *50*, 571-581.
- Chester, F.M., and J.M. Logan (1986), Implications for mechanical properties of brittle faults from observation of the Punchbowl fault zone, California, *Pageoph.* *124*, 79-106.
- Chester, F.M., J.M. Chester, D.L. Kirschner, S.E. Schulz, and J.P. Evans (2004), Structure of large-displacement, strike-slip fault zones in the brittle continental crust, in *Rheology and Deformation of the Lithosphere at Continental Margins*, edited by G. D. Karner, J.D. Morris, N.W. Driscoll, and E.A. Silver, Columbia University Press, New York, New York, 223-260.
- Deere, D.U. and D.W. Deere (1987), The Rock Quality Designation (RQD) index in practice, *ASTM Spec. Tech. Publ.*, *984*, 91-101.
- Eberhart-Phillips, D.M. D.H. Han, and M.D. Zoback (1989), Empirical relationships among seismic velocity, effective pressure, porosity, and clay content in sandstone, *Geophysics*, *54*, 82-89.
- Eberhart-Phillips, D. and A. J. Michael (1998), Seismotectonics of the Loma Prieta, California, region determined from three-dimensional V_p , V_p/V_s , and seismicity, *J. Geophys. Res.*, *103*, 21099–21120.
- Erickson, S. G., Deformation of shale and dolomite in the Lewis thrust fault zone, northwestern Montana, U. S. A. , *Can. Jour. Earth Sci.*, *31*, 1440-1448, 1994.
- Evans, J. P., and F. M. Chester, 1995, Fluid-rock interaction in faults of the San Andreas system; inferences from San Gabriel Fault rock geochemistry and microstructures. *J. Geophys. Res.*, *100*, 13007-13020.
- Evans J. P., C. B. Forster, and J. V. Goddard, (1997), Permeability of fault-related rocks, and implications for hydraulic structure of fault zones, *J. Struct. Geol.*, *19*, 1393-1404.
- Faulkner, D. C., A. C. Lewis, E. H. Rutter, (2003) On the internal structure and mechanics of large strike-slip fault zones; field observations of the Carboneras Fault in southeastern Spain, *Tectonophysics*. *367*, 235-251.
- Forster, C.B., J.P. Evans, K. Wantanabe, H. Tanaka, R. Jeffreys, and T. Nohara (2003), Hydrological properties and structure of the Mozumi Fault, central Japan, *Geophys. Res. Lett.* *30*(6), doi: 10.1029/2002GL014904.
- Fujita, M. (2002), A new contribution to the stratigraphy of the Tetori Group, adjacent to Lake Kuzuryu, Fukui Prefecture, central Japan, *Mem. Fukui Pref. Dinosaur Mus.*, *1*, 41-53.
- Gettemy, G. L., H. J. Tobin, J. A. Hole, and A. Y. Sayed, (2004), Multi-scale compressional wave velocity structure of the San Gregorio fault zone, *Geophys. Res. Lett.*, *31*, doi: 10.1029/2003GL018826.
- Goddard, J.V., and J.P. Evans (1995), Chemical changes and fluid-rock interaction in faults of crystalline thrust sheets, northwestern Wyoming, U.S.A., *J. Struct. Geol.*, *17*, 533-547.
- Gutscher, M. (2001), An Andean model of interplate coupling and strain partitioning applied to the flat subduction zone of SW Japan (Nankai Trough), *Tectonophysics*, *33*, 95-109.
- Gutscher, M., and S. Lallemand (1999), Birth of a major strike-slip fault in SW Japan, *Terra Nova*, *11*, 203-209.
- Haas, C.J. (1981), Static Stress-Strain Relationships, in *Physical Properties of Rocks and Minerals*, edited by Y. S. Touloukian, W. R. Judd and R. F. Roy, *II-2*, McGraw-Hill, Columbus, Ohio, 409-489.
- Hamada, G.M. (2004), Reservoir fluids identification using V_p/V_s ratio, *Oil Gas Sci. Tech.*, *59*, 649-654.
- Hardebeck, J. L., A. J. Michael, T. M. Brocher (2007), Seismic velocity structure and seismotectonics of the eastern San Francisco bay region, California, *Bull. Seismol. Soc. Am.*, *97*(3), doi:10.1785/0120060032.
- Hatheway, A.W., and G.A. Kiersch (1989), Engineering Properties of Rock, in *Practical Handbook of Physical Properties of Rocks and Minerals*, edited by R.S. Charmichael , CRC Press, Boca Raton, Florida, 672-715.
- Heermance, R. V., Z. K. Shipton, and J. P. Evans, (2003) Fault structure control on fault slip and ground motion during the 1999 rupture of the Chelungpu fault, Taiwan , *Bull. Seis. Soc. Am.* *93*, p. 1034-1050.
- Hirahara, K., Y. Ooi, M. Ando, K. Haso, Y. Wada, and T. Ohkura (2003), Dense GPS Array observations across the Atotsugawa fault, central Japan, *Geophys. Res. Lett.*, *30*(6), doi: 10.1029/2002GL015035.
- Holland, M., J. L., Urai, W. van der Zee, H. Stanjek, and J. Konstanty, J., (2006) Fault gouge evolution in highly overconsolidated claystones, *J. Struct. Geol.*, *28*, 323-332.

- Ito, H. (1999), Studies on Fault Activity at the Atotsugawa Fault – Is the Atotsugawa Fault Creeping? *Geol. Surv. Japan Info. Circ.* S-12.
- Ito, H. (2003), Detailed seismicity and crustal structure in the Atotsugawa fault, a partly creeping fault, central Honshu, Japan, in *Intn'l Union Geod. Geophys. 2003 Scientific Program*, 30 June to 11 July 2003, Sapporo, Japan.
- Keller, J.V.A., S. H. Hall, C. J. Dart, K. R. McClay, (1995). The geometry and evolution of a transpressional strike-slip system: the Carboneras fault, SE Spain. *J. Geol. Soc. Lon.* 152, 339– 351.
- Klimentos, T., and C. McCann, 1990, Relationships among compressional wave attenuation, porosity, clay content, and permeability in sandstones, *Geophysics*, 55, 998-1014.
- Kramer, S.L. (1996), Earthquakes and Wave Propagation, in *Geotechnical Earthquake Engineering*, Prentice-Hall, Upper Saddle River, New Jersey, 18-53 and 143-183.
- Lee, H.K., and H.S. Kim (2005), Comparison of structural features of the fault zone developed at different protoliths: crystalline rocks and mudrocks, *J. Struct. Geol.*, 27,2099-2112.
- Li, Y.G., K. Aki, J.E. Vidale, and F. Xu, (1999), Shallow structure of the Landers fault zone from explosion-generated trapped waves. *J. Geophys. Res.*, 104, 20,257-20,275.
- Li, Y.G., J.E. Vidale, D.D. Oglesby, S.M. Day, and E. Cochran, (2003), Multiple fault rupture of the M7.1 Hector Mine, California, earthquake from fault zone trapped waves, *J. Geophys. Res.*, 108, 2165, doi:10.1029/2001JB00145.
- Li, Y.G., J.E. Vidale, and E.S. Cochran, (2004), Low-velocity damaged structure of the San Andreas Fault at Parkfield from fault zone trapped waves, *Geophys. Res. Lett.*, 31(12), L12S06, doi:10.1029/2003GL019044.
- Li, Y. G., and Vidale, J. E, 1996, Low-velocity fault-zone guided waves: Numerical Investigations of trapping efficiency, *Bull. Seis. Soc. Am.*, 86, 371-378.
- Mamada, Y., Y. Kuwahara, H. Ito, and H. Takenaka (2002), 3-D finite-difference simulation of seismic fault zone waves, Application to the fault zone structure of the Mozumi-Sokenobu fault, central Japan, *Earth Plan. Space*, 54, 1055-1058.
- _____, 2004, Discontinuity of the Mozumi-Sukenobu fault low-velocity zone, central Japan, inferred from 3-D finite-difference simulation of seismic fault zone waves excited by explosive sources, *Tectonophysics*, 378, 209-222.
- Matsuda, T. (1966), Strike-slip faulting along the Atotsugawa fault, Japan (in Japanese with English summary), *Bull. Earth. Res. Inst.*, 44, 1179-1212.
- Matsuda, T., and Y. Kinugasa (1991), Active faults in Japan, *Episodes*, 14, 199-204.
- Mariko, T., M. Kawada, M. Miura, and S. Ono, (1996), Ore formation processes of the Mozumi skarn-type Pb-Zn-Ag deposits in the Kamioka Mine, Gifu Prefecture, central Japan; a mineral chemistry and fluid inclusion study Shigen Chishitsu, (*Resource Geology*) 46, 337-354.
- Mavko, G., M. Tapan, and J. Dvorkin (1998), *The Rock Physics Handbook; tools for seismic analysis in porous media*, Cambridge Univ. Press, Cambridge, United Kingdom, 329 pp.
- McGuire, J., and Y. Ben-Zion (2005), High-resolution imaging of the Bear Valley section of the San Andreas Fault at seismogenic depths with fault-zone head waves and relocated seismicity, *Geophys. Jour. Int.*, 163, 152-164.
- Mikumo, T., H. Wada, and M. Koizumi (1988), Seismotectonics of the Hida region, central Honshu, Japan, *Tectonophysics*, 147, 95-119.
- Mizuno, T., K. Nishigama, H. Ito, and Y. Kuwahara (2004), Deep structure of the Mozumi-Sukenobu fault, central Japan, estimated from the subsurface array observation of fault zone trapped waves, *Geophys. J. Int.*, 159, 622-642.
- Nohara, T., H. Tanaka, K. Watanabe, N. Furukawa, and A. Takami, (2006), In situ hydraulic tests in the active fault surge tunnel, Kamioka mine, excavated through the active Mozumi-Sukenobu fault zone and their hydrogeological significance, *Island Arc*, 15, 527-545.
- Ohtani, T., K. Fujimoto, H. Ito, H. Tanaka, N. Tomida, and T. Higuchi (2000), Fault rocks and past to recent fluid characteristics from the borehole survey of the Nojima Fault ruptured in the 1995 Kobe earthquake, Southwest Japan, *J. Geophys. Res.*, 105, 16,161-16,171.
- Rutter, E.H., Maddock, R.H., Hall, S.H., White, S.H., 1986. Comparative microstructures of natural and experimentally produced clay-bearing fault gouges. *Pure Appl. Geophys.* 124, 3 – 30.
- Sagiya, T., S. Miyasaki, and T. Tada (2000), Continuous GPS array and present-day crustal deformation of Japan, *Pure Appl. Geophys.*, 157, 2303-2322.

- Sayed, A.Y. (2001), In Situ compressional wave velocity across an exposed brittle fault zone, Master's thesis, 40 pp., Polytechnic Institute and State University, Blacksburg, Virginia.
- Schulz, S.E. and J.P. Evans (2000), Mesoscopic structure of the Punchbowl Fault, Southern California, and the geologic and geophysical structure of active strike-slip faults, *J. Struct. Geol.*, 22, 913-930.
- Shingu K., T. Okada, A. Saitou, K. Wada, K. Horinokuchi, and T. Nakajima (1997), Study using a drift in the active fault zone (in Japanese with English abstract), PNC TJ1174 97-001.
- Shibley, T. H., G. F. Moore, J. J. Tobin, and J. C. Moore, (1997), Synthesis of the Barbados decollement seismic reflection response from drilling-based geophysical observations and physical properties, in: Shibley, T. H., Y. Ogawa, P. Blum, and J. M. Bahr, eds., Proc. Ocean Drilling Prog, Scientific Results, 156, 293-302.
- Spudich, P. and K. B. Olsen (2001), Fault zone amplified waves as a possible seismic hazard along the Calaveras Fault in Central California, *Geophys. Res. Lett.*, 28, 2533-2536.
- Stanchits, S.A., D.A. Lockner, and A.V. Ponomarev (2003), Anisotropic changes in P-wave velocity and attenuation during deformation and fluid infiltration of granite, *Bull. Seis. Soc. Am.*, 93, 1803-1822.
- Stierman, D.J., and R.L. Kovach (1979), An *in situ* velocity study: The Stone Canyon Well, *J. Geophys. Res.*, 84, 672-678.
- Szwilski, A.B. (1982), Determination of elastic modulus of stress relief cores of shale, *ASTM Geotech. Testing J.*, 5, 34-41.
- Taira, A. (2001), Tectonic evolution of the Japanese island arc system, *Ann. Rev. Earth Plan.*, 29, 109-134.
- Takeuchi, A., and H. Ongirad (2003), Recurrence interval of big earthquakes along the Atotsugawa fault system, central Japan: Results of seismo-geological survey, *Geophys. Res. Lett.*, 30(6), doi: 10.1029/2002GL014957.
- Thurber, C. H. Zhang, F. Waldhauser, J. Hardebeck, A. Michael, and D. Eberhart-Phillips (2006), Three dimensional compressional wavespeed model, earthquake relocations, and focal mechanisms for the Parkfield, California, region, *Bull. Seismol. Soc. Am.*, 96(4B), S38-S49, doi: 10.1785/0120050825.
- Tobin, H. J., and J. C. Moore, (1997), Variations in ultrasonic velocity and density with pore press in the decollement zone, northern Barbados ridge accretionary prism, in: Shibley, T. H., Y. Ogawa, P. Blum, and J. M. Bahr, eds., Proc. Ocean Drilling prog., Scientific Results, 156, 125-135.
- Udias, A. (1999), Anelasticity and Anisotropy, in *Principles of Seismology*, Cambridge University Press, Cambridge, United Kingdom, 253-273.
- Wada, H., T. Mikumo, and M. Koizumi (1990), Recent seismic activity in the northern Hida, Toyama Bay and Noto Peninsula regions, Kyoto Daigaku Bosai Kenkyujo Nenpo, *Disaster Prev. Res. Inst. Ann.*, 33, Kyoto University, Kyoto, Japan, 57-74.
- Wang, Z., and Nur, A., 1990, Wave velocities in hydrocarbon-saturated rocks: experimental results, *Geophysics*, 55, 723-733.
- Warr, L. N., and S. Cox, Clay mineral transformation and weakening mechanisms along the Alpine fault, New Zealand, in: Holdsworth, R. E., Strachan, R. A., Magloughlin, J. F., and Knipe, R. J., (eds.), The nature and tectonic significance of fault zone weakening, *Geol. Soc. Lond. Spec. Pub.* 186, 103-112, 2001.
- Wibberley, C. A. J., and T. Shimamoto, 2003, Internal structure and permeability of major strike-slip fault zones: the Median Tectonic line in Mie Prefecture, southwestern Japan, *J. Struct. Geol.*, 25, 59-78.
- Wilson, J. E., J. S. Chester, F. M. Chester, 2003, Microfracture analysis of fault growth and wear processes, Punchbowl fault, San Andreas system, California, *J. Struct. Geol.*, 25, 1855-1873.
- Wong, T., C. David, and W. Zhu (1997), The transition from brittle faulting to cataclastic flow in porous sandstones: Mechanical deformation, *J. Geophys. Res.*, 102, 3009-3025.
- Yamaji, A. (1994), An introduction to the Cenezoic tectonics of the Japan arc, *Geofisica Internacional*, 33, 21-14.
- Yamaji, A. (2003), Slab rollback suggested by latest Miocene to Pliocene forearc stress and migration of volcanic front in southern Kyushu, northern Ryukyu Arc, *Tectonophysics*, 364, 9-24.
- Yan, Y., B. A. van der Pluijm, and D. R. Peacor, Deformation microfabrics of clay gouge, Lewis Thrust, Canada: a case for fault weakening from clay transforation, in: Holdsworth, R. E., Strachan, R. A., Magloughlin, J. F., and Knipe, R. J., (eds.), The nature and tectonic significance of fault zone weakening, *Geol. Soc. Lond. Spec. Pub.*, 112-124, 2001.

Figure Captions

Figure 1. Generalized geology surrounding the Atotsugawa, Mozumi, and Ushikubi faults, Japan [Atotsugawa Fault System]. The Active Fault Survey Tunnel [AFST] intersects the Mozumi fault where it cuts Jurassic-Cretaceous Tetori Group sandstone and shale (map modified from Matsuda, 1966). Inset map shows the location of the area.

Figure 2. Geologic map of the Active Fault Survey Tunnel, and detailed core log from borehole A. This map is extracted from a 1:500 map created by geologists of the Mitsui Mining and Smelting Company in 1997 along the tunnel walls and supplemented by core logs of the boreholes. Lithologies and structures are shown as described by the mine geologists. Borehole A is inclined 60° to N 24° W, and sample locations and lithology within the box have been projected to the horizontal. Samples discussed in this study are from borehole A. All samples collected in borehole A are siltstone. Sample MZ-1, collected from borehole 1, is siltstone protolith. Data from boreholes 1 and 2, shown in figure 3, cut both of the major fault zones. The lithologic log is an expansion of the region sampled across the main portion of the fault zone, and the stratigraphy is expanded. The map presents the data from mine geologists; the stratigraphic log is based on detailed observations of the core.

Figure 3. Rock quality descriptor [RQD] and core recovery for boreholes 1 and 2. A. Borehole 1 crosses the southern fault strand and incorporates a zone of intact rock next to a region of highly fractured rocks in the fault. B. Data for borehole 2 which crosses the zone interpreted to be the main fault zone. RQD, core recovery, and water fluxes mark the fault zone.

Figure 4. Lower hemisphere equal area stereonet of contoured poles to fracture planes recorded along borehole A of the Active Fault Survey Tunnel (data presented in tables in Shingu et al., 1997). The orientation of borehole A and the Mozumi fault within the Active Fault Survey Tunnel are also shown for reference. Fracture set 1 has a mean orientation of 155° , 20° W. Fracture set 2 has a mean orientation of 001° , 71° E. Fracture set 3 has a mean orientation of 063° , 74° S.

Figure 5. Wireline logs, sample positions, and correlated and interpreted lithology of borehole A (Shingu et al., 1997).

Figure 6. Histograms of the distribution of experimentally-derived values for Young's Modulus (E) and Poisson's Ratio (ν) for sandstone, shale, and siltstone, and calculated values for Mozumi fault rock samples. Data on claystone are very limited, thus values are simply listed. The calculated value for the protolith (samples MZ-1 and MZ-1A) of the Mozumi fault zone is indicated by the purple bar. The experimental data come from works referenced in Haas (1981).

* = complete overlap of blue and red bars.

Figure 7. Representation of select properties across the Mozumi fault zone and properties of the protolith [MZ-1]. Stars show the location of samples used in this study. General lithology is shown at the bottom of the page with sh = shale and ss = sandstone. Red lines indicate the locations of clay gouge. Roman numerals indicate the degree of damage as assigned by mining geologists with I having the least damage and III having the most damage. The scales for each bar graph are based on typical maximums and minimums, as well as the range of values for Mozumi fault rocks (Castagna et al., 1985), with the exception of clay amount, which is based on the values of Mozumi fault rocks and protolith so that the changes across the fault zone can be more easily observed.

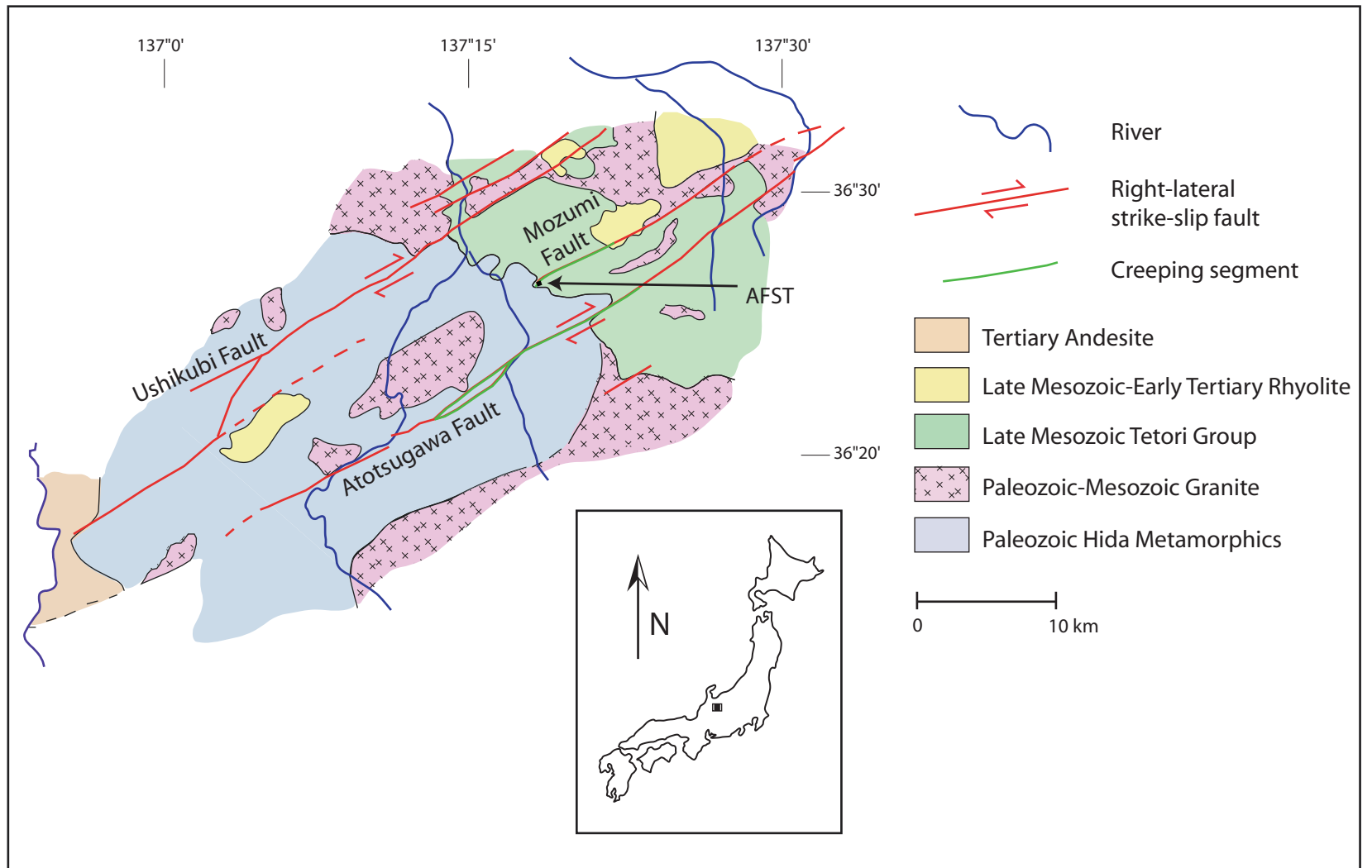
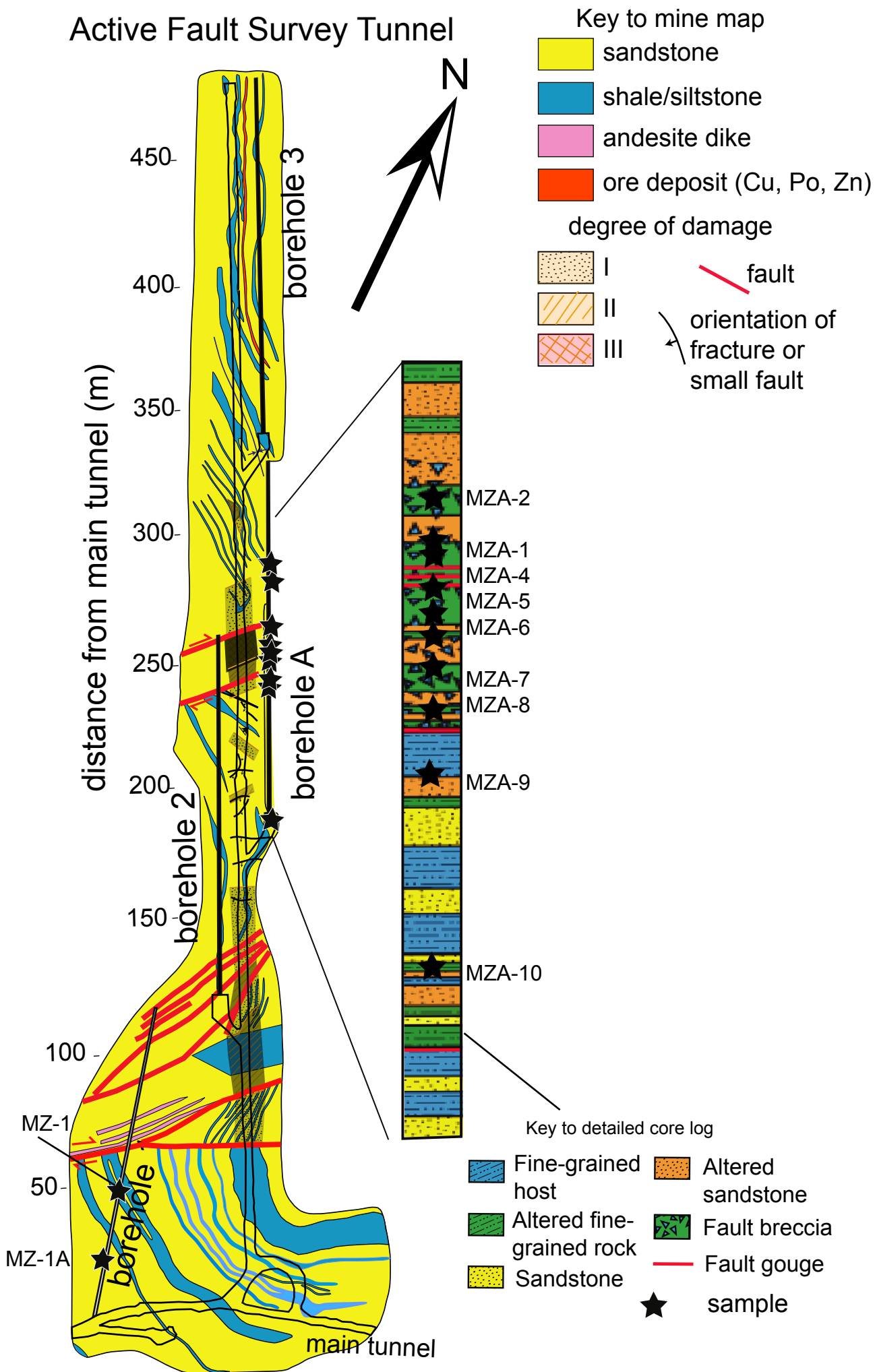


Figure 1.

Active Fault Survey Tunnel



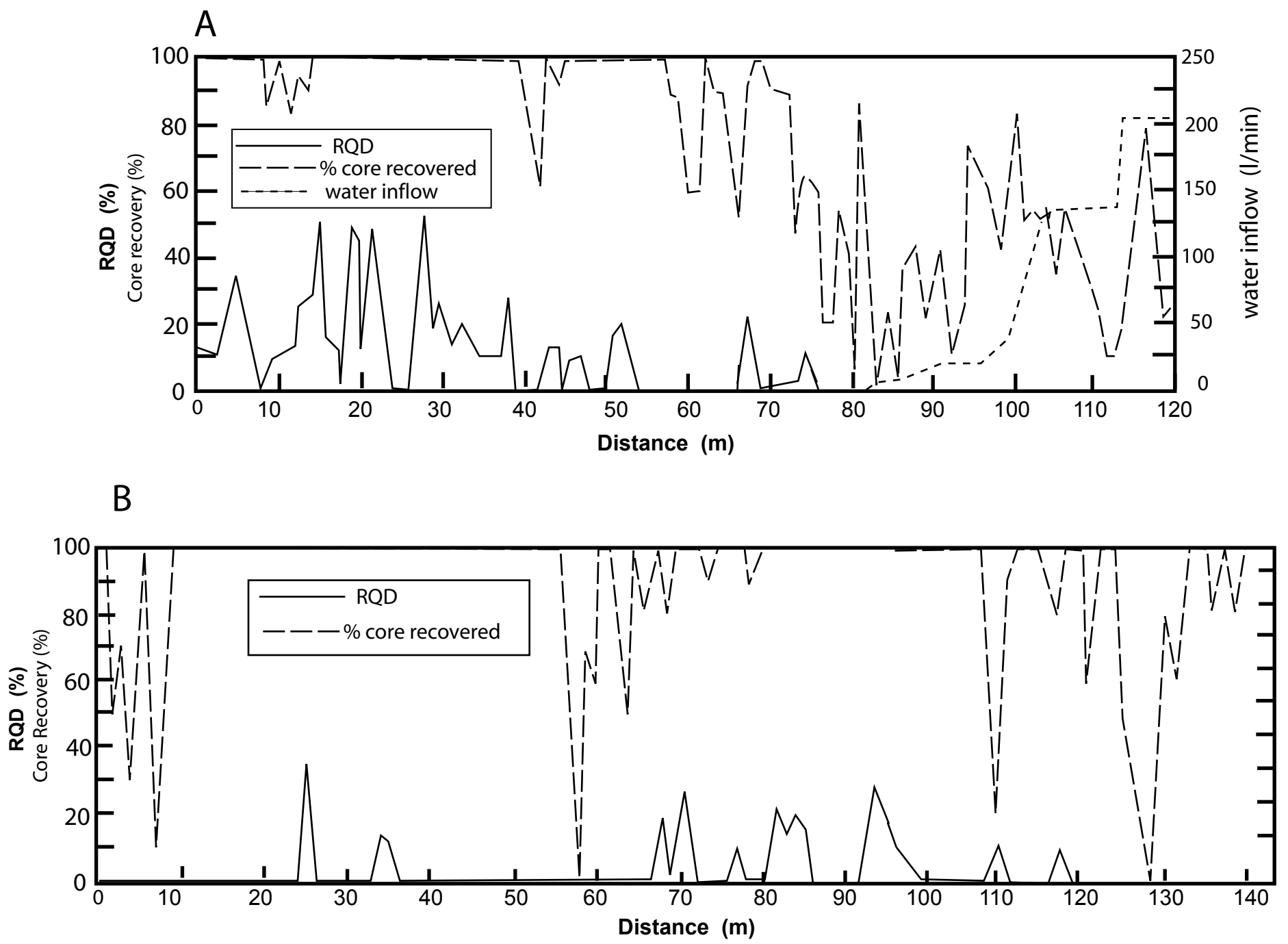


Figure 3

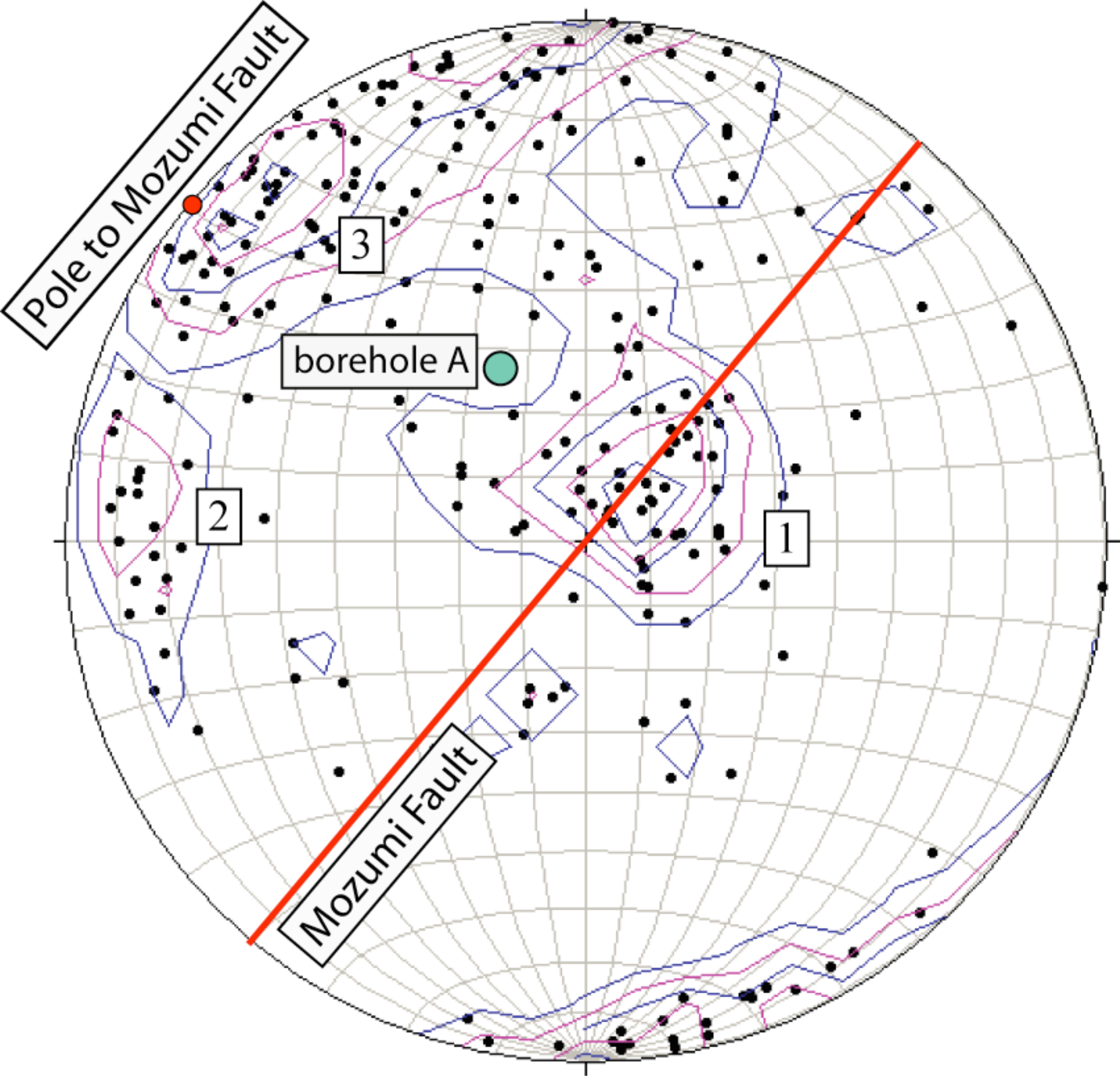


Figure 4.

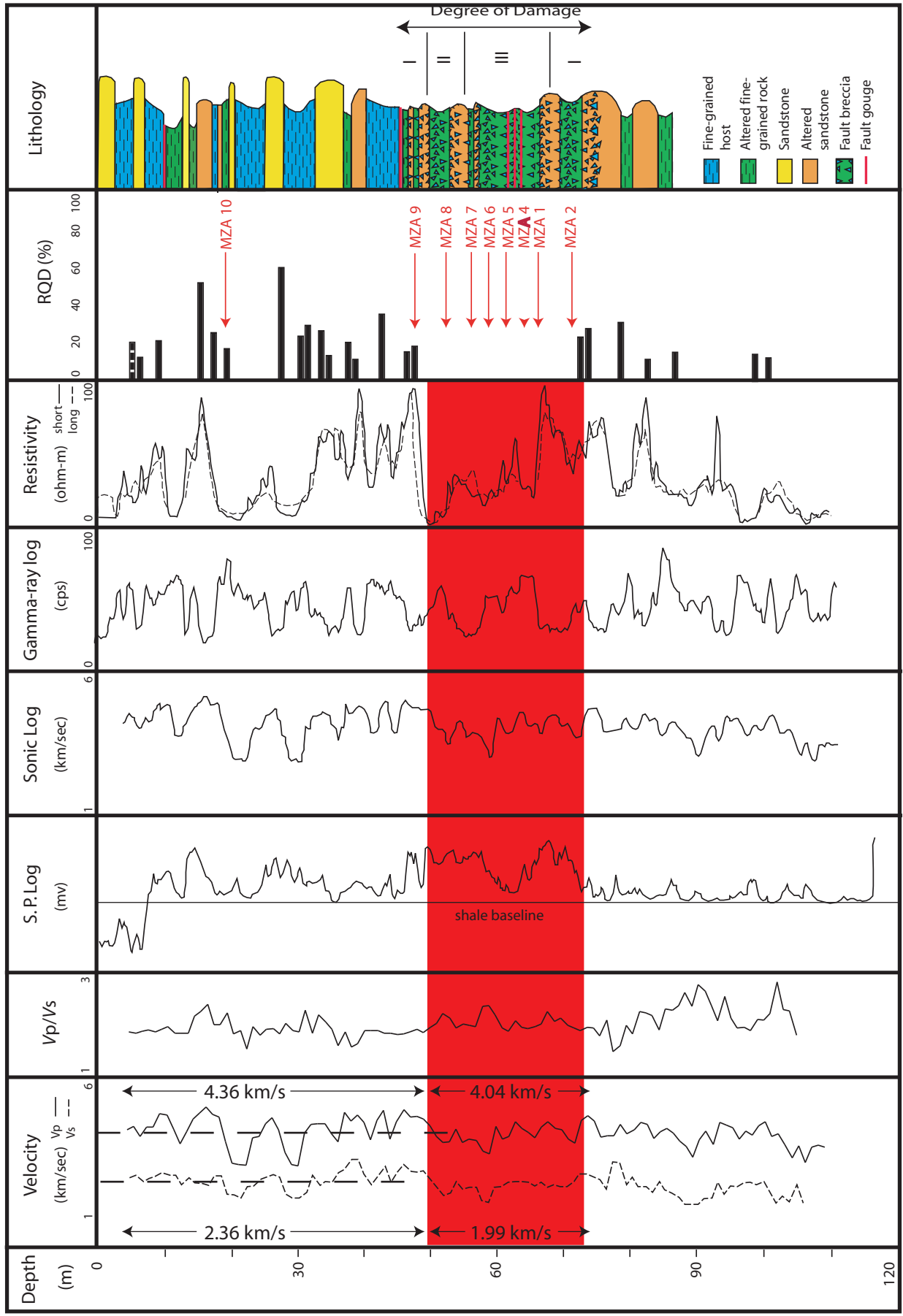


Figure .5

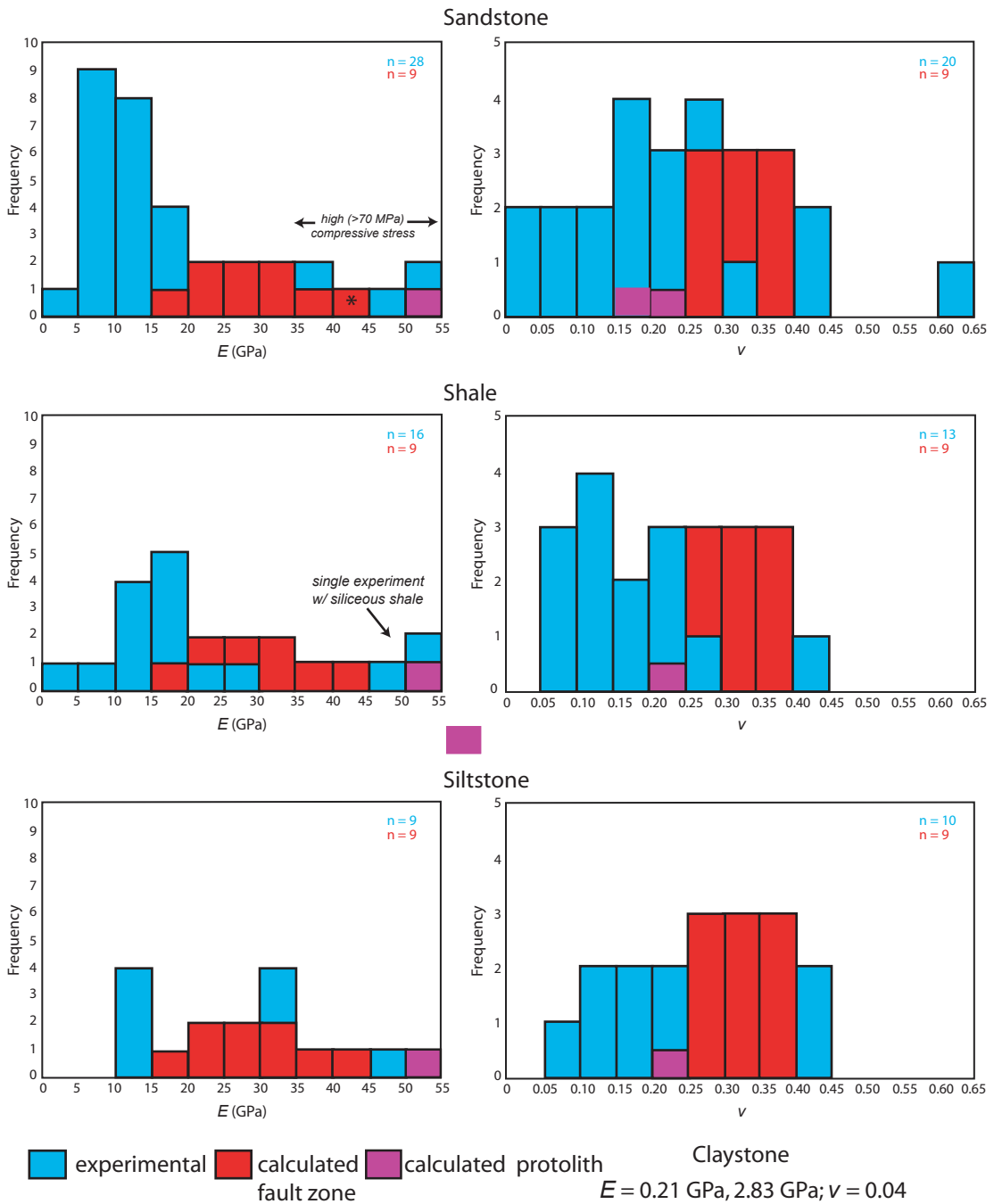


Figure 6

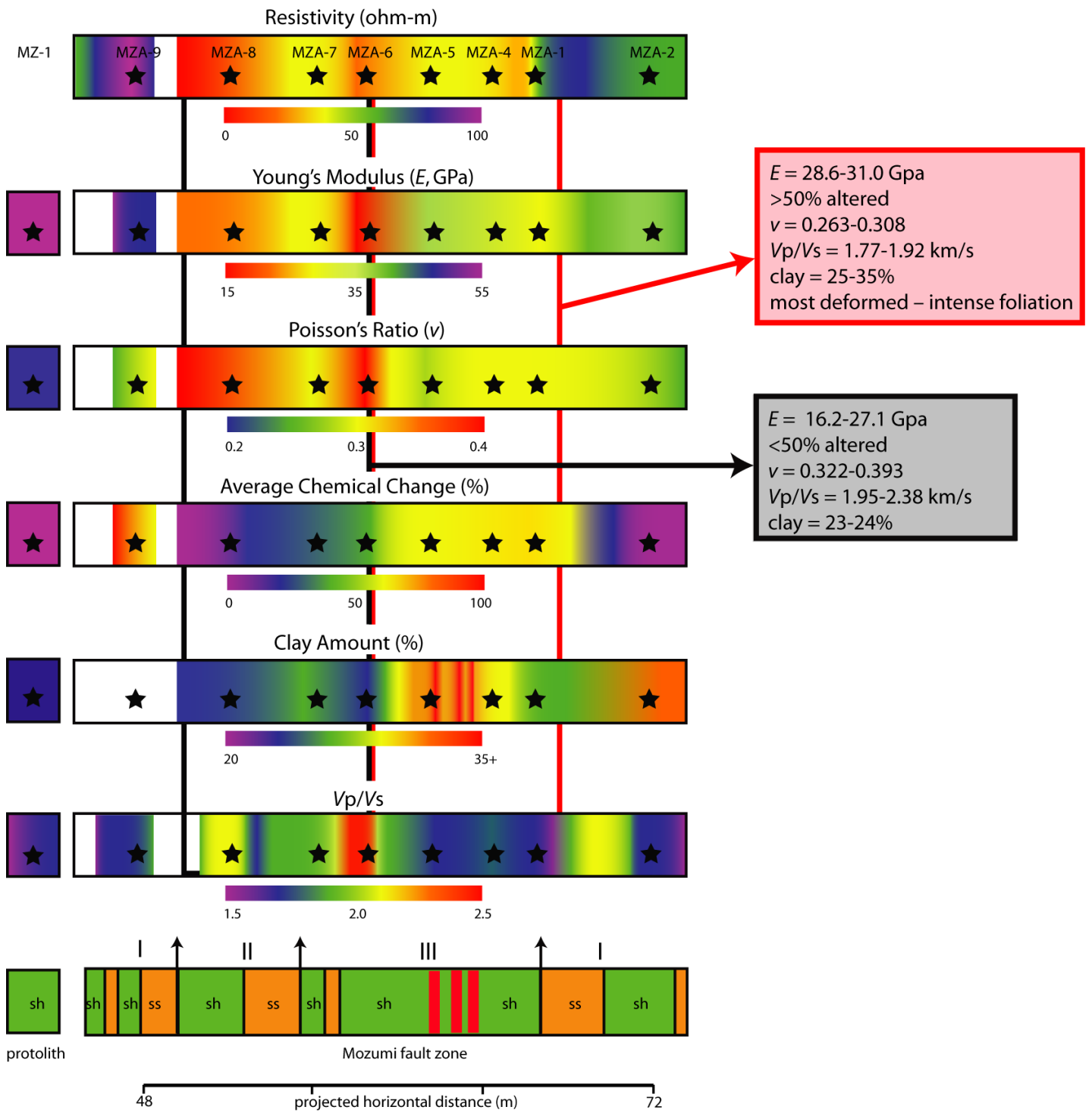


Figure 11

Table 1

Descriptions of samples from the Mozumi fault zone used in this study including distances along the borehole and projected horizontal distances from the southeast end of borehole A.

Sample	Description	Distance along borehole (m)	Horizontal distance (m)
MZA-2	Siltstone fault breccia, abundant clay, intensely foliated matrix and shear fabric	143.2	71.6
MZA-1	Siltstone fault breccia, abundant clay, crenulation foliation in matrix, hematite and debris-filled fractures	133	66.5
MZA-4	Siltstone fault breccia, abundant clay, calcite and quartz veins, intensely foliated matrix	128.4	64.2
MZA-5	Siltstone fault breccia, abundant clay, intensely foliated matrix and shear fabric	122.4	61.2
MZA-6	Siltstone fault breccia, moderately foliated, shear fabrics	116.57	58.3
MZA-7	Siltstone fault breccia, abundant clay, intensely foliated matrix and shear fabric	111.76	55.9
MZA-8	Siltstone, angular fault breccia, calcite veins, fractures, anastomosing brown clay	104.8	52.4
MZA-9	Altered siltstone cut by subsidiary fault, indurated and mineralized siltstone against weak clay-rich fault rock	95.75	47.9
MZA-10	Siltstone, fault with clay gouge, quartz and calcite veins	38.2	19.1

Table 2

Estimated values for properties of Mozumi fault rocks including density [ρ], seismic wave velocities [V_s , V_p], calculated physical, and calculated mechanical properties for borehole A samples and a protolith sample from borehole 1, as well as permeability and porosity values from Forster et al. (2003).

Sample	ρ (g/cc)	v_s (km/s)	v_p (km/s)	μ (g/cm-sec ²)	λ (g/cm-sec ²)	Calculated E (GPa)	Calculated ν	V_p/V_s	Calculated Porosity (%) [5],[6]	Permeability (m ²), connected porosity (%) of Forster et al. (2003)
MZA-2	2.77	2.20	4.16	1.34*10 ¹¹	2.11*10 ¹¹	35.0	0.306	1.89	10, 11	3.7 E ⁻¹⁵ , 8.0
MZA-1	2.49	2.13	3.76	1.13*10 ¹¹	1.26*10 ¹¹	28.6	0.264	1.77	17, 16	1.9 E ⁻¹⁵ , 8.4
MZA-4	2.33	2.25	4.31	1.18*10 ¹¹	1.97*10 ¹¹	31.0	0.263	1.92	-	5.3 E ⁻¹⁵ , 9.0
MZA-5	2.80	2.05	3.90	1.18*10 ¹¹	1.90*10 ¹¹	30.9	0.308	1.90	14, 14	1.6 E ⁻¹⁵ , 7.2
MZA-6	2.87	1.45	3.45	6.03*10 ¹⁰	2.21*10 ¹¹	16.2	0.393	2.38	22, 20	
MZA-7	2.56	2.00	3.90	1.02*10 ¹¹	1.85*10 ¹¹	27.1	0.322	1.95	15, 15	
MZA-8	2.60	1.75	3.83	7.96*10 ¹⁰	2.22*10 ¹¹	21.8	0.368	2.19	16, 16	
MZA-9a	2.66	2.55	4.76	1.73*10 ¹¹	2.57*10 ¹¹	44.9	0.299	1.87	-	
MZA-9b	2.41	2.55	4.76	1.57*10 ¹¹	2.32*10 ¹¹	40.8	0.298	1.87	-	
MZA-10	2.84	1.70	3.79	8.21*10 ¹⁰	2.44*10 ¹¹	22.6	0.374	2.23	18, 17	
Borehole 1 protolith										
MZ-1	2.85	2.80	4.75	2.23*10 ¹¹	2.10*10 ¹¹	55.4	0.242	1.70	4, 6	4.0 E ⁻¹⁷ , 1.6
MZ 1A	2.83	2.91	4.83	2.34*10 ¹¹	2.27*10 ¹¹	57.3	0.19	1.71	7	
Additional samples from Forster et al. (2003)										
MZA-143.2 (breccia)									3.7 E ⁻¹⁵ , 8.0	
MZA-127.8 (clay gouge)									2.2 E ⁻¹⁶ , 11.1	
"clay-rich zones"									E ⁻¹⁸ – E ⁻¹⁹	

Table 3
Hydrometer results for percent clay analysis.

Sample	Sample Weight	40 sec	Temp.	Corrected Hydrometer	6 hr 40 sec	Temp.	Corrected Hydrometer	% Clay (±4%)
MZA-10	40	11.0	26	13.16	7.0	23	8.08	20
MZA-8	40	14.0	25	15.80	8.0	23	9.08	23
MZA-7	40	14.0	25	15.80	8.5	23	9.58	24
MZA-6	40	13.0	25	14.80	8.0	23	9.08	23
MZA-5	40	16.5	25	18.30	10.0	23	11.80	28
MZA-2	30	12.5	25	14.30	8.0	23	9.08	30
MZA-1	40	16.5	25	18.30	9.0	23	10.08	25
MZ-1	35	12.5	25	14.30	7.0	23	8.08	23
Control	40	3.0	26	5.16	3.0	23	4.08	14

Table 4

P-wave and S-wave velocities for borehole A by rock type, and average P-wave velocities for the Mozumi fault zone and wall rock. Typical ranges of v_p and v_s for sandstones, shaley rocks, and “mudrocks” are listed (Castagna et al., 1985).

Lithology	v_p (km/s)		v_s (km/s)	
	range	average	range	average
sandstone	3.64-5.41	4.62	1.52-2.86	2.25
mixed sandstone/shale	4.35-4.76	4.56	2.44-2.56	2.50
shale	3.70-5.26	4.24	1.85-2.50	2.19
siltstone	3.08-5.26	4.42	1.28-3.13	2.16
clay	3.33-3.85	3.59	1.67-1.69	1.68
average		4.49		2.21

average v_p of wall rock	4.36	average v_p of MF zone	4.04
average v_s of wall rock	2.36	average v_s of MF zone	1.99
typical range for v_p	3.0-5.0	typical range for v_s	1.5-2.5